Joint Localization and Synchronization Using Space-Based SOOP: Theory and Experiments

Mei Leng, Wee Peng Tay, François Quitin, Chi Cheng, Sirajudeen Gulam Razul, and Chong Meng Samson See

Abstract

We consider the problem of tracking a receiver using signals-of-opportunity (SOOPs) from beacons and a reference anchor with known positions and velocities, and where all devices have asynchronous local clocks or oscillators. We model the clock drift at individual devices by a two-state model with unknown clock offset and clock skew, and analyze the biases introduced by clock asynchronism in the received signals. Based on an extended Kalman filter, we propose a sequential estimator to jointly track the receiver location, velocity, and its clock parameters using time-difference-of-arrival and frequency-difference-of-arrival measurements obtained from the SOOP samples collected by the receiver and a reference anchor. Field experiments are carried out using a software defined radio testbed, and Iridium satellites as the SOOP beacons. Experiment and simulation results demonstrate that our measurement model has a good fit, and our proposed estimator can successfully track both the receiver location, velocity, and the relative clock offset and skew with respect to the reference anchor with good accuracy.

Index Terms

geo-localization, synchronization, signal-of-opportunity, EKF, USRP

I. INTRODUCTION

A signal-of-opportunity (SOOP) refers to a public signal broadcast from an established transmitting infrastructure for non-navigation purposes. Such signals conform to well-established standards and are present in most urban areas with relatively high signal-to-noise ratio (SNR). SOOP beacons

F. Quitin, Cheng Chi and W.P. Tay are with the Nanyang Technological University, Singapore. (e-mail:{fquitin, chengchi, wptay}@ntu.edu.sg).

M. Leng, C.M. Samson See and S.G. Razul are with Temasek Laboratories@NTU (TL@NTU), Singapore. (e-mail: {lengmei, samsonsee, ESirajudeen}@ntu.edu.sg).

can be both land-based stations and space-based transmitters. Examples of land-based beacons include AM/FM radio signal transmission stations [1], terrestrial television broadcast masts [2]–[4], cellular communication base stations [5]–[7], and WiFi access points [8]–[10]. Space-based beacons include commercial planes (each transmits an automatic dependent surveillance-broadcast (ADS-B) signal [11]), and various space satellites like low Earth orbit (LEO) satellites, including the Iridium satellites used for communication purposes [12], [13]. Depending on their signal characteristics and transmitter properties, various SOOP signals have proved to be useful alternatives to the use of Global Navigation Satellite Systems (GNSS) for navigation services [13], and in applications like sensor networks to provide location information in order for the networks to correctly interpret the sensory data [14]–[16]. As most GNSS are medium earth orbit systems, their SNRs are lower than that of typical SOOP, and do not penetrate well into buildings or through other obstacles. Navigation services based on GNSS are therefore usually only available when there is a clear sky view. However, since GNSS signals are designed to provide localization information, they are more informative and typically yield better location estimates than using SOOPs alone [17]–[19]. In the case where not enough GNSS satellites are in line of sight, SOOPs can help to augment GNSS localization. In some scenarios, GNSS may be completely unavailable. For example, since GNSS techniques have become mature, it is likely that GNSS signals may be jammed or disabled by adversaries during war time [20]. Therefore, navigation using SOOPs has gained increasing interest recently [3], [7], [17], [21].

Since SOOPs have not been designed for navigation purposes, and SOOP beacons act as uncooperative broadcast anchors, it may be difficult to have a priori knowledge of the signal structure and certain signal characteristics like transmit power and transmit time. Therefore, typical localization metrics that can be extracted from a SOOP are limited to received signal strength and angle-of-arrival at a single receiver, and time-difference-of-arrival (TDOA) and frequency-difference-of-arrival (FDOA) of the same signal between two receivers. Compared with the first two metrics, which have poor measurement accuracies in cluttered environments [22], [23], TDOA and FDOA are attractive alternatives, since they can remove the ambiguity caused by unknown transmit time or unknown signal structure, and are somewhat more robust as biases caused by clutters tend to cancel each other out if the two receivers are relatively close to each other. Therefore, we focus on TDOA and FDOA measurements in this paper. In [17], we proposed an estimator using differential TDOA (DTDOA) and FDOA, where the location and velocity of every receiver are estimated using measurements from at least 5 beacons simultaneously in 2D space. In this paper, we consider a

more practical situation where only one beacon is available per TDOA and FDOA measurement period, and the receiver location and velocity are estimated sequentially.

In general, land-based SOOP beacons are typically stationary, and their precise locations are known. However, their coverage areas are smaller than those of the space-based systems, which have near-global coverage in many instances. The signal qualities of land-based beacons are also lower due to more severe multipath effects in ground-to-ground communications in an urban environment. In this paper, we focus on space-based systems. We use Iridium satellites as beacons in our empirical experiments, and obtain the beacon position and velocity from the SGP4 models [24]. The positioning errors of the SGP4 models are known to range from 2 km to 10 km [25], which leads to significant localization errors if no other reference anchors are used. Therefore, in this paper, we consider the case where the position and velocity of one receiver is known a priori and serves as a reference anchor to help another receiver perform state estimation using the SOOP. The use of an anchor as a localization aid also applies to the scenario in which a receiver is navigating in an urban canyon while the anchor could be a static node positioned on top of a building with good GNSS coverage, or an unmanned aerial vehicle that has access to accurate location information.

The most critical challenge for receiver position and velocity estimation using TDOA and FDOA measurements is synchronization between the two receivers. An offset between the local clocks of the receivers introduces biases into TDOA measurements, for which even a microsecond offset significantly degrades the overall estimation performance. Likewise, a relative clock skew between the two receivers distorts the FDOA measurements. In order to obtain reliable timing and frequency information, it is essential that receivers are time synchronized and achieve precise frequency alignment, and therefore most existing methods make this simplifying assumption (see [7], [26] and the references therein). However, clock synchronization is difficult to achieve and maintain in practice [27], [28]. Moreover, in order not to interfere with the existing operations of SOOP beacons, localization using SOOP often requires that SOOP beacons do not need to be aware of the presence of the receivers using their signals, and will not actively synchronize with them or provide a common clock reference for the receivers.

In the context of wireless sensor networks, it has been proposed to jointly estimate sensors' positions and clock drifts so that localization and synchronization can be achieved simultaneously. Following [29], this problem has received considerable attention. The paper [30] considers localization for a single receiver using signals from multiple synchronized beacons, while [31] and [19]

investigate a more general case where a set of anchor nodes cooperate with each other to localize a single transmitter. The work [32] considers a similar source localization problem using TOA measurements with the transmit time being an unknown parameter. These works consider a static target and require certain prior knowledge such as the transmit signal [30], [31] and transmit time stamp [32]. Another major difference with our work is that they require the receiver or transmitter to cooperate with the anchor transmitters or receivers, which is unrealistic for localization using SOOPs. The localization of mobile nodes was considered in [33], but it again requires cooperation amongst transmitters and receivers.

The use of TDOA and FDOA measurements for localization has been investigated in [34], [35], which proposed to localize a transmitter with asynchronous receivers. One crucial assumption in these works is that biases due to clock drifts are modeled as constant error terms in both TDOA and FDOA measurements. In [35], it is also assumed the receiver has prior knowledge of the transmission signal as well as its periodicity. The following natural and important questions were left unanswered:

- Is it accurate to model clock drifts as constant error terms in the TDOA and FDOA measurements?
- How can we obtain TDOA and FDOA measurements with minimum prior knowledge from SOOP beacons?
- Can we sequentially perform joint localization and synchronization using SOOP measurements?

In this paper, we answer the above three important questions through theoretical analysis and empirical experiments. We assume that a target receiver and a reference anchor receive signals from the same SOOP beacons, where the reference anchor is a receiver node with known location and velocity. (We relax this assumption in our simulations and experiments where the location and velocity of the anchor are estimated up to an unknown error.) We also assume that all devices, including the receiver, anchor, and beacons, are asynchronous. Our main contributions are the following:

- We propose an anchor-aided localization scheme using SOOPs. The proposed scheme assumes minimum prior knowledge of the SOOP beacons, and it is sufficient for both the receiver and anchor to know only the nominal transmission frequency,[1] signal bandwidth, position and

[1]The nominal transmission frequency refers to the publicized frequency a SOOP beacon is supposed to transmit at. However, due to local clock drifts, the actual transmission frequency may be different from the nominal frequency.

velocity of each beacon. For space-based beacons like satellites, the location and velocity of the beacons can be calculated using the SGP4 model [24].

- We derive closed-form expressions for TDOA and FDOA measurements under clock asynchronism. We show that the bias introduced in the TDOA measurement is a time-varying term that depends linearly on the clock offsets and clock skews of the receiver and anchor. The bias in the FDOA measurement can be approximated as the relative clock skew between the receiver and anchor (i.e., a clock parameter that describes the speed of receiver clock drift relative to that of the anchor). Empirical experiments using a software defined radio testbed and the Iridium satellites as SOOP beacons verifies the correctness of our measurement model.
- Using TDOA and FDOA measurements between the receiver and anchor, we propose a sequential estimator to jointly track the the location, velocity, and clock parameters of the receiver, with respect to (w.r.t.) the anchor. Empirical experiments using our software defined radio platform and simulation results demonstrate that our proposed algorithm can correctly track the clock drift dynamics, with receiver location and velocity estimation performance approaching the Cramér-Rao bound (CRB). In our empirical experiment where the receiver and anchor are on average 40 km apart and using the SOOP from a single Iridium satellite at each TDOA and FDOA measurement period, our proposed algorithm can localize a static receiver with mean estimation error less than 40 meters, and track a moving receiver with mean estimation error less than 100 meters. These errors are consistent with those predicted by the CRB.

The rest of this paper is organized as follows. In Section II, we present our model assumptions and propose an anchor-aided localization scheme. In Section III, we analyze the distortion caused by clock offsets and drifts to the received signal, obtain approximate closed-form expressions for TDOA and FDOA estimates, and propose a sequential estimator for jointly estimating the receiver's location, velocity, and clock parameters. In Section IV, we present empirical and simulation results, and we conclude in Section V.

Notations: We use bold faced upper-case letters to represent matrices and bold faced lower-case letters for vectors. The transpose and the conjugate transpose of $\mathbf{A}$ are denoted as $\mathbf{A}^T$ and $\mathbf{A}^H$, respectively. We use $\cdot^{(l)}$ to indicate that the parameter is specific to the l-th observation period. The operator $\mathbb{E}$ denotes mathematical expectation. The real multivariate Gaussian distribution with mean $\boldsymbol{\mu}$ and covariance $\mathbf{P}$ is denoted by $\mathcal{N}(\boldsymbol{\mu}, \mathbf{P})$. The complex multivariate Gaussian distribution with mean $\boldsymbol{\mu}$ and covariance $\mathbf{P}$ is denoted by $\mathcal{CN}(\boldsymbol{\mu}, \mathbf{P})$.

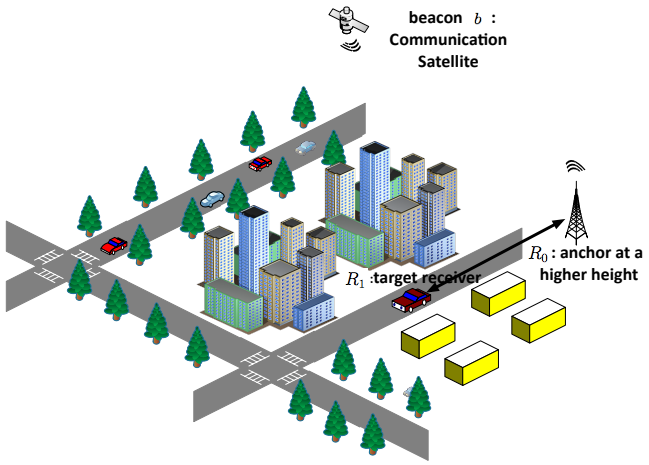

Fig. 1. Localization using space-based SOOP beacon b in urban environments.

II. System Model

We consider the problem of localizing and tracking a receiver R_1 using the SOOP from a set $\mathcal{B}$ of space-based beacons. The receiver performs self-localization and velocity estimation with the aid of a reference anchor R_0 within communication range. We assume that the receiver and anchor receive signals from the same beacon during each TDOA and FDOA measurement throughout the whole observation period of the receiver. An example scenario is shown in Figure 1, where a beacon $b \in \mathcal{B}$ has known position $\mathbf{p}_b$ and velocity $\mathbf{v}_b$, and broadcasts signals at a nominal carrier frequency f_b. We investigate a general scenario where the following assumptions hold.

Assumption 1

(i) The receiver and anchor can differentiate signals from different beacons, and have prior knowledge of each beacon's location, velocity, and nominal transmit frequency.

(ii) The anchor can communicate its location and velocity to the receiver.

(iii) The clock offset between the receiver and anchor is sufficiently small so that the measurement period of any beacon signal at the receiver overlaps with that at the anchor.

Assumption 1(i) can be satisfied by allowing the receiver and anchor to first learn about their operating environment with preloaded beacon information. For example, Iridium satellites are LEO satellites using a hybrid time division multiple access / frequency division multiple access (TDMA/FDMA) architecture. In total, 252 frequency access channels are available, each satellite has a known Earth coverage area at any given time, and its orbital trajectory can be predicted

using the SGP4 or SDP4 model [24]. Hence, a receiver with prior knowledge of the region it is in, can first perform a spectrum scan to detect signals from different channels, and then identify the satellite by cross checking the satellites whose coverage regions currently intersect the region the receiver is in. With the satellites identified, a receiver that has the SGP4 model programmed in advance can calculate the satellites' positions and velocities at any given time.

For Assumption 1(iii), it is sufficient to coarsely synchronize the receiver and anchor to within an accuracy on the order of a second. The local clocks of the receiver and anchor are then allowed to drift. Generally, oven-controlled crystal oscillator (OCXO) drifts with a clock skew ranging from 10^{-11} to 10^{-6} [36], and a clock offset of about 86.4 ms is accumulated in one day in the worst case.

We assume that SOOPs are ad hoc, and may not be received at regular intervals. In Section III-C, we discuss how the receiver state estimation accuracy is related to how frequently a SOOP is detected. Each time a SOOP is detected, the receiver and anchor both sample over a fixed time interval, and store the samples for TDOA and FDOA computations. We call this an observation period. The integration time [37] used to compute the TDOA and FDOA is then not more than the length of each observation period. An anchor-aided localization scheme can be conducted as follows:

(i) The receiver detects available beacons and exchanges beacon information with an anchor in its communication range. To initiate the localization and velocity estimation procedure, the receiver and anchor agrees on the start time of receiving the signal via handshaking.

(ii) After recording signal samples from the same set of beacons in each observation period, the anchor forwards its signal samples to the receiver, which utilizes them to compute TDOA and FDOA. A similar scheme was proposed in [18], which aims to localize a group of automated robots. In this paper, we focus on how to design a sequential algorithm to jointly track the receiver and estimate its clock drift parameters.

We perform empirical experiments using Iridium satellites as the beacons in Section IV, but our proposed algorithm is not limited to Iridium satellites. We also note that our algorithm is applicable to land-based SOOP beacons with line of sight to the receiver and anchor.

A. Distorted received signal for asynchronous receivers

We assume that each receiver conducts in total L observations sequentially. The l-th observation starts at nominal receive time $t^{(l)}$ and lasts for $T_e^{(l)}$ second, and obviously we have $t^{(1)} < t^{(2)} <$

$\cdots < t^{(L)}$. In order to infer its location, the target receiver R_1 extracts TDOA and FDOA from signals received by itself and the anchor R_0 in each observation period. Since all receivers are asynchronous, the measurements are distorted due to the local oscillator biases, and it is important to analyze how such distortions affect the TDOA and FDOA measurements.

To begin with, we adopt the commonly used two-state clock model [38], [39] which describes the local oscillator with a clock skew and a clock offset [40]. Consider the l-th observation period. For the beacon b, let its clock skew be $\beta_b^{(l)}$ and its clock offset be $\Omega_b^{(l)}$. The clock skew $\beta_b^{(l)}$ characterizes the rate of clock drift and is typically related to the systematic and slowly varying frequency error due to aging and the environment. The clock offset $\Omega_b^{(l)}$ characterizes any clock drifts accumulated up to time $t^{(l)}$.

Since space-based beacons are equipped with high quality oscillators, their clock skew residual, i.e., $\left|\beta_b^{(l)} - 1\right|$, are stable from 10^{-12} to 10^{-10}, which accumulates at most 86.4 ns per day and hence can be neglected. Therefore, we model the local time for beacon b by

$$t_b(t) = t + \Omega_b^{(l)}. \tag{1}$$

Let $s_b(t)$ be the nominal baseband signal at beacon b. The transmitted passband signal $u_b(t)$ is

$$u_b(t) = s_b(t + \Omega_b^{(l)}) \exp\{\mathrm{i}2\pi f_b(t + \Omega_b^{(l)})\}, \tag{2}$$

where $\mathrm{i} = \sqrt{-1}$ and $t \in [t^{(l)}, t^{(l+1)}]$.

On the other hand, receivers are generally equipped with low-cost oscillators, such as OCXO and temperature compensated crystal oscillator (TCXO), which typically have the clock skew residual in parts per million (ppm, 10^{-6}), and we model the local time for the receiver j by

$$t_j(t) = t^{(l)} + \beta_j^{(l)}(t - t^{(l)}) + \Omega_j^{(l)}, \tag{3}$$

where clock skew $\beta_j^{(l)}$ and clock offset $\Omega_j^{(l)}$ are w.r.t. time $t^{(l)}$.

When two receivers have agreed to sample beacon b's signal starting at time $t^{(l)}$ for a period of $T_e^{(l)}$ seconds, the actual receiving time at receiver R_j is given by $\hat{t}_j^{(l)} = t^{(l)} - \Omega_j^{(l)}/\beta_j^{(l)}$ and the actual observation duration will be $T_e^{(l)}/\beta_j^{(l)}$ due to the local clock drift. As the signal travels from beacon b to receiver R_j, we define the instantaneous time delay and Doppler shift at time $t^{(l)}$ as,

$$\text{time delay: } \mathcal{T}_{j,b}^{(l)} = \frac{\left\|\mathbf{p}_j^{(l)} - \mathbf{p}_b^{(l)}\right\|}{c}, \tag{4}$$

$$\text{Doppler shift: } \mathcal{D}_{j,b}^{(l)} = -\frac{f_b}{c}\left(\mathbf{v}_j^{(l)} - \mathbf{v}_b^{(l)}\right)^T \mathbf{u}_{j,b}^{(l)}. \tag{5}$$

The constant c is the speed of light, $\mathbf{u}_{j,b}^{(l)}$ is the direction from beacon b to receiver j at time $t^{(l)}$ defined as

$$\mathbf{u}_{j,b}^{(l)} = \frac{\mathbf{p}_j^{(l)} - \mathbf{p}_b^{(l)}}{\left\| \mathbf{p}_j^{(l)} - \mathbf{p}_b^{(l)} \right\|}, \tag{6}$$

and $\mathbf{p}_\bullet^{(l)}$ and $\mathbf{v}_\bullet^{(l)}$ represent the location and velocity of the corresponding device at time $t^{(l)}$. Assuming that the observation duration $T_e^{(l)}$ in the l-th observation period is short enough so that the relative movement between R_j and beacon b is small, we have the channel impulse response as [41],

$$h_{j,b}^{(l)}(t) \approx \delta(\gamma_{j,b}^{(l)}(t - \hat{t}_j^{(l)} - \eta_{j,b}^{(l)}) + \hat{t}_j^{(l)}), \tag{7}$$

where $\eta_{j,b}^{(l)} = \mathcal{T}_{j,b}^{(l)}$ and $\gamma_{j,b}^{(l)} = 1 + \mathcal{D}_{j,b}^{(l)}/f_b$.

Therefore, for the l-th observation period, the noise-free received signal at R_j has the baseband representation

$$r_{j,b}^{(l)}(t) = \exp\{-\mathrm{i}2\pi f_b \beta_j^{(l)} t\} \int_{\hat{t}_j^{(l)}}^{\hat{t}_j^{(l)} + T_e^{(l)}/\beta_j^{(l)}} u_b(t-\tau) h_{j,b}^{(l)}(\tau) \mathrm{d}\tau. \tag{8}$$

Substituting (7) into (8), we can write the received baseband signal as $r_{j,b}^{(l)}(t) \propto s_b(\gamma_{j,b}^{(l)}(t - \hat{t}_j^{(l)} - \eta_{j,b}^{(l)}) + \hat{t}_j^{(l)} + \Omega_b^{(l)}) \exp\Big\{\mathrm{i}2\pi f_b(\gamma_{j,b}^{(l)} - \beta_j^{(l)})t\Big\}$ for $t \in [\hat{t}_j^{(l)}, \hat{t}_j^{(l)} + T_e^{(l)}/\beta_j^{(l)}]$. Let T_s be the nominal sampling interval, the sample sequence at sensor j can be obtained as

$$r_{j,b}^{(l)}[n] = r_{j,b}^{(l)}\left(t/\beta_j^{(l)}\right)|_{t=nT_s}. \tag{9}$$

The scaling factor $1/\beta_j^{(l)}$ captures the effect of the free-running local oscillator at R_j. Let $\mathbf{r}_{j,b}^{(l)}$ be the corresponding sample sequence, it follows from (9) that

$$\mathbf{r}_{j,b}^{(l)} \propto\!\!\!\!\sim\; s_b\left(\mathbf{n} - \eta_{j,b}^{(l)} + \Omega_b^{(l)}\right) \exp\Big\{\mathrm{i}2\pi f_b(\gamma_{j,b}^{(l)} - \beta_j^{(l)})\mathbf{n}\Big\}, \tag{10}$$

where $\propto\!\!\!\!\sim$ means approximately proportional to, and $\mathbf{n} = (\lceil t/(\beta_j^{(l)} T_s)\rceil T_s : t \in [\hat{t}_j^{(l)}, \hat{t}_j^{(l)} + T_e^{(l)}/\beta_j^{(l)}])$ is the time index sequence. Therefore, the received signal during the l-th observation period can be approximately characterized by its time delay, frequency offset, and clock biases at time $t^{(l)}$ when the observation duration $T_e^{(l)}$ is short enough. For the L observation periods, all noise-free received signal sample sequences are denoted as $\{\mathbf{r}_{j,b}^{(l)}\}_{l=1,\cdots,L}$. Suppose that the received signal at receiver R_j, $j = 0, 1$, is corrupted by white Gaussian noise $\boldsymbol{\varpi}_j^{(l)} \sim \mathcal{CN}(\mathbf{0}, \mathbf{C}_j)$, we denote the received signal at R_j as $\tilde{\mathbf{r}}_{j,b}^{(l)} = \mathbf{r}_{j,b}^{(l)} + \boldsymbol{\varpi}_j^{(l)}$ for $l = 1, \cdots, L$.

III. JOINT LOCALIZATION AND SYNCHRONIZATION ALGORITHM

A. TDOA and FDOA measurements

The receiver R_1 can obtain the approximate TDOA and FDOA w.r.t. the anchor R_0 of the SOOP from beacon b by maximizing the amplitude of the cross ambiguity function $\mathcal{A}(\tau,\xi) = \sum_n \tilde{\mathbf{r}}_{1,b}^{(l)}[n]\tilde{\mathbf{r}}_{0,b}^{(l)*}[n-\tau]\exp\{-\mathrm{i}2\pi\xi n\}$ of their respective received signals from beacon b. Let $\tau_b^{(l)}$ be the estimated TDOA multiplied by the speed of light c, and $\xi_b^{(l)}$ be the estimated FDOA multiplied by $-c/f_b$ for the l-th observation time slot. It can be shown that

$$\begin{aligned}
\tau_b^{(l)} &= c[\beta_1^{(l)}\eta_{1,b}^{(l)} - \beta_0^{(l)}\eta_{0,b}^{(l)} + \beta_1^{(l)}\Omega_b - \beta_0^{(l)}\Omega_b + (\hat{t}_0^{(l)} + T_e^{(l)}/\beta_0^{(l)}) - (\hat{t}_1^{(l)} - T_e^{(l)}/\beta_1^{(l)})] \\
&= \beta_1^{(l)}\left\|\mathbf{p}_1^{(l)} - \mathbf{p}_b^{(l)}\right\| - \beta_0^{(l)}\left\|\mathbf{p}_0^{(l)} - \mathbf{p}_b^{(l)}\right\| \\
&\quad + c\left[\left(\frac{1}{\beta_0^{(l)}} - \frac{1}{\beta_1^{(l)}}\right)T_e^{(l)} + \frac{\Omega_1^{(l)}}{\beta_1^{(l)}} - \frac{\Omega_0^{(l)}}{\beta_0^{(l)}} + (\beta_1^{(l)} - \beta_0^{(l)})\Omega_b^{(l)}\right] + \varpi_b^{\tau}, \qquad (11a) \\
\xi_b^{(l)} &= -c[(\gamma_{1,b}^{(l)} - \beta_1^{(l)})/\beta_1^{(l)} - (\gamma_{0,b}^{(l)} - \beta_0^{(l)})/\beta_0^{(l)}] \\
&= \frac{1}{\beta_1^{(l)}}\left(\mathbf{v}_1^{(l)} - \mathbf{v}_b^{(l)}\right)^T\mathbf{u}_{1,b}^{(l)} - \frac{1}{\beta_0^{(l)}}\left(\mathbf{v}_0^{(l)} - \mathbf{v}_b^{(l)}\right)^T\mathbf{u}_{0,b}^{(l)} + c\left(\frac{1}{\beta_0^{(l)}} - \frac{1}{\beta_1^{(l)}}\right) + \varpi_b^{\xi}, \qquad (11b)
\end{aligned}$$

where the clock parameters $\beta_j^{(l)}$ and $\Omega_j^{(l)}$ are the clock skew and offset of receiver R_j at time $t^{(l)}$, respectively. We also let ϖ_b^{τ} and ϖ_b^{ξ} be measurement noises, which are assumed to be zero-mean and independent Gaussian random variables for all $b \in \mathcal{B}$.

We can rewrite (11) as

$$\begin{aligned}
\tau_b^{(l)} &= \left\|\mathbf{p}_1^{(l)} - \mathbf{p}_b^{(l)}\right\| - \left\|\mathbf{p}_0^{(l)} - \mathbf{p}_b^{(l)}\right\| + \left(\frac{1}{\beta_0^{(l)}} - \frac{1}{\beta_1^{(l)}}\right)cT_e^{(l)} + \underbrace{\left[\frac{\Omega_1^{(l)}}{\beta_1^{(l)}} - \frac{\Omega_0^{(l)}}{\beta_0^{(l)}} + \left(\beta_1^{(l)} - \beta_0^{(l)}\right)\Omega_b^{(l)}\right]c}_{\triangleq\theta^{(l)}} \\
&\quad + \underbrace{\varpi_b^{\tau} + (\beta_1^{(l)} - 1)\left\|\mathbf{p}_1^{(l)} - \mathbf{p}_b^{(l)}\right\| - (\beta_0^{(l)} - 1)\left\|\mathbf{p}_0^{(l)} - \mathbf{p}_b^{(l)}\right\|}_{\approx\varpi_b^{\tau}}, \qquad (12a) \\
\xi_b^{(l)} &= \left(\mathbf{v}_1^{(l)} - \mathbf{v}_b^{(l)}\right)^T\mathbf{u}_{1,b}^{(l)} - \left(\mathbf{v}_0^{(l)} - \mathbf{v}_b^{(l)}\right)^T\mathbf{u}_{0,b}^{(l)} + \left(\frac{1}{\beta_0^{(l)}} - \frac{1}{\beta_1^{(l)}}\right)c \\
&\quad + \underbrace{\varpi_b^{\xi} + \left(\frac{1}{\beta_1^{(l)}} - 1\right)\left(\mathbf{v}_1^{(l)} - \mathbf{v}_b^{(l)}\right)^T\mathbf{u}_{1,b}^{(l)} - \left(\frac{1}{\beta_0^{(l)}} - 1\right)\left(\mathbf{v}_b^{(l)} - \mathbf{v}_0^{(l)}\right)^T\mathbf{u}_{0,b}^{(l)}}_{\approx\varpi_b^{\xi}}. \qquad (12b)
\end{aligned}$$

The approximations are due to the fact that the clock skew residuals, $\left|\beta_j^{(l)} - 1\right|$, $j = 0, 1$, are typically very small (several ppm), and introduce errors far smaller than the measurement noises.

Let $\alpha^{(l)} = c(1/\beta_0^{(l)} - 1/\beta_1^{(l)})$. It follows from (12) that

$$\tau_b^{(l)} \approx \left\|\mathbf{p}_1^{(l)} - \mathbf{p}_b^{(l)}\right\| - \left\|\mathbf{p}_0^{(l)} - \mathbf{p}_b^{(l)}\right\| + T_e^{(l)}\alpha^{(l)} + \theta^{(l)} + \varpi_b^{\tau}, \tag{13a}$$

$$\xi_b^{(l)} \approx (\mathbf{v}_1^{(l)} - \mathbf{v}_b^{(l)})^T \mathbf{u}_{1,b}^{(l)} - (\mathbf{v}_0^{(l)} - \mathbf{v}_b^{(l)})^T \mathbf{u}_{0,b}^{(l)} + \alpha^{(l)} + \varpi_b^{\xi}. \tag{13b}$$

The bias $\theta^{(l)}$ in (13a) corresponds to the clock offset accumulated up to time $t^{(l)}$. Assuming that clocks are drifting slowly and the interval between two consecutive observations is short, i.e., $\beta_j^{(l)} \approx \beta_j^{(l-1)}$, it is easy to show that $\theta^{(l)} \approx \theta^{(l-1)} + (t^{(l)} - t^{(l-1)})\alpha^{(l-1)}$, which implies that the bias in the TDOA measurement is a time-varying term that depends linearly on the relative clock skew between two receivers. This is in contrast to the models in [34], [35], which assume that the TDOA error is constant. In our model, a larger error will also be accumulated over a longer observation period.

In Section IV, our field experiments demonstrate that (13) captures the biases caused by asynchronous clocks and correctly describes the distorted TDOA and FDOA measurements. A similar measurement model was derived in [17], and a robust algorithm against clock biases was proposed to estimate the locations and velocities of both receivers. But [17] considered a batch processing method and assumes that beacons transmit simultaneously, which is equivalent to having $L = 1$ and $t^{(l)} = 0$ for all measurements in (13a). In practice, this assumption may not hold. For example, beacons like the Iridium satellites and GSM base stations adopt TDMA schemes, making it difficult to receive SOOPs from multiple different beacons in the same short observation period. The receiver hardware implementation is also more complex if it is required to listen to multiple SOOPs at the same time. In this paper, we consider a more practical situation where one burst from one beacon is transmitted per time slot, and design a *sequential* estimator for the receiver.

For the l-th observation period, the target receiver R_1 collects one pair of measurements $\{\tau_b^{(l)}, \xi_b^{(l)}\}$ and the corresponding beacon states $\{\mathbf{p}_b^{(l)}, \mathbf{v}_b^{(l)}\}$. Without loss of generality, when multiple beacons are available in one time slot, it is equivalent to stacking all measurements into a vector. The target receiver then seeks to jointly estimate its state $\{\mathbf{p}_1^{(l)}, \mathbf{v}_1^{(l)}\}$ and its clock parameters $\{\theta^{(l)}, \alpha^{(l)}\}$ relative to the anchor R_0. In the following, we propose a sequential algorithm for this estimation problem.

Remark 1: The exchange of received signals can be done by using a frequency mixer with a direct amplify-and-forward operation, which translates the received analog signal at the anchor to a different frequency band that does not interfere with the beacon's transmission. This requires a minimum level of processing at the anchor side. However, when spectrum is scarce, it is possible for

the anchor to transmit only limited information if it knows the pulse shape and modulation scheme of the beacon. This can be done by first obtaining a bit sequence through blind demodulation, reconstructing a local version of the beacon signal with the bit sequence, and estimating time-of-arrival (TOA) and frequency-of-arrival (FOA) by cross-correlating the received signal with the reconstructed signal. The anchor then broadcasts its estimated TOA and FOA values. A similar approach was applied in [11] for ADS-B signal. In our experiments, we have used Iridium satellites as SOOP beacons. Since we know that Iridium satellites are transmitting signals using DE-QPSK modulation and raised-cosine pulse shaping, we can also apply the above local processing method. Our experimental results showed a similar performance compared to directly cross-correlating the received signals at both R_0 and R_1.

B. Sequential joint localization and synchronization

Our objective is to estimate the locations and velocities of the mobile receiver R_1. We collect all unknowns and measurements in the l-th observation period into vectors $\mathbf{x}^{(l)} \triangleq [(\mathbf{p}_1^{(l)})^T, (\mathbf{v}_1^{(l)})^T, \theta^{(l)}, \alpha^{(l)}]^T$ and $\mathbf{y}^{(l)} \triangleq [\tau_b^{(l)}, \xi_b^{(l)}]^T$. In the Bayesian framework, we view the state of $\mathbf{x}^{(l)}$ as a random variable, and the tracking problem is to recursively estimate $\mathbf{x}^{(l)}$ given the measurement $\mathbf{y}^{(1:l)}$ up to time $t^{(l)}$ by maximizing the posterior probability $p\left(\mathbf{x}^{(l)} \middle| \mathbf{y}^{(1:l)}\right)$. Computing $p\left(\mathbf{x}^{(l)} \middle| \mathbf{y}^{(1:l)}\right)$ involves two steps: prediction and update, as follows [42]:

1) prediction:

$$p\left(\mathbf{x}^{(l)} \middle| \mathbf{y}^{(1:l-1)}\right) = \int p\left(\mathbf{x}^{(l)} \middle| \mathbf{x}^{(l-1)}\right) p\left(\mathbf{x}^{(l-1)} \middle| \mathbf{y}^{(1:l-1)}\right) \mathrm{d}\mathbf{x}^{(l-1)}, \tag{14}$$

2) update:

$$p\left(\mathbf{x}^{(l)} \middle| \mathbf{y}^{(1:l)}\right) \propto p\left(\mathbf{y}^{(l)} \middle| \mathbf{x}^{(l)}\right) p\left(\mathbf{x}^{(l)} \middle| \mathbf{y}^{(1:l-1)}\right). \tag{15}$$

The probability density function $p\left(\mathbf{y}^{(l)} \middle| \mathbf{x}^{(l)}\right)$ describes the relationship between the measurement $\mathbf{y}^{(l)}$ and the state $\mathbf{x}^{(l)}$ at the l-th observation period, while $p\left(\mathbf{x}^{(l)} \middle| \mathbf{x}^{(l-1)}\right)$ shows how the state $\mathbf{x}^{(l)}$ evolves over time.

Following (13), we define the measurement model as

$$\underbrace{\begin{bmatrix} \tau_b^{(l)} \\ \xi_b^{(l)} \end{bmatrix}}_{\mathbf{y}^{(l)}} = \underbrace{\begin{bmatrix} \left\| \mathbf{p}_1^{(l)} - \mathbf{p}_b^{(l)} \right\| + T_e^{(l)} \alpha^{(l)} + \theta^{(l)} \\ (\mathbf{v}_1^{(l)} - \mathbf{v}_b^{(l)})^T \mathbf{u}_{1,b}^{(l)} + \alpha^{(l)} \end{bmatrix} - \begin{bmatrix} \left\| \mathbf{p}_0^{(l)} - \mathbf{p}_b^{(l)} \right\| \\ (\mathbf{v}_0^{(l)} - \mathbf{v}_b^{(l)})^T \mathbf{u}_{0,b}^{(l)} \end{bmatrix}}_{\triangleq \mathbf{g}_b(\mathbf{x}^{(l)})} + \boldsymbol{\varpi}^{(l)}. \tag{16}$$

Assuming the measurement noise $\boldsymbol{\varpi}^{(l)}$ is a zero mean Gaussian random variable with variance $\mathbf{R}_l$, we have

$$p\left(\mathbf{y}^{(l)}\middle|\,\mathbf{x}^{(l)}\right) \propto \exp\{-\frac{1}{2}(\mathbf{y}^{(l)}-\mathbf{g}_b(\mathbf{x}^{(l)}))^T\mathbf{R}_l^{-1}(\mathbf{y}^{(l)}-\mathbf{g}_b(\mathbf{x}^{(l)}))\}.$$

The noise covariance matrix $\mathbf{R}_l$ depends on the estimation accuracy for TDOA and FDOA measurements. It was shown in [37], [43] that their CRBs can be obtained in closed form and are fully determined by quantities related to signal characteristics like effective SNR, integration time, and signal bandwidth.

The dynamic model on the other hand requires a certain level of prior information about the unknown state. The clock state in our case is relatively simple due to the fact that general oscillators can be characterized with a constant clock skew for a short period. Defining the observation interval as $\Delta_l \triangleq t^{(l)} - t^{(l-1)} \geq T_e^{(l)}$, and following from the discussion after (13), we have

$$\begin{bmatrix}\theta^{(l)}\\ \alpha^{(l)}\end{bmatrix} = \begin{bmatrix}1 & \Delta_l\\ 0 & 1\end{bmatrix}\begin{bmatrix}\theta^{(l-1)}\\ \alpha^{(l-1)}\end{bmatrix} + \boldsymbol{\nu}_c^{(l)}, \tag{17}$$

where $\boldsymbol{\nu}_c^{(l)}$ models the clock errors in the l-th observation period. It is well known that the clock errors can be suitably modelled by a stochastic processes characterizing the evolution of several clock error components [39], [44]. Following from [39], we consider three clock error components, including phase noise, frequency noise, and the time variation of clock skew. Each component can be readily modelled as a Wiener process, and we define σ_Ω, σ_β, and σ_d as the diffusion coefficients which gives the intensity of each noise. We have $\boldsymbol{\nu}_c^{(l)} \sim \mathcal{N}\left(0, \mathbf{Q}_c^{(l)}\right)$ with

$$\mathbf{Q}_c^{(l)} = \begin{bmatrix}\sigma_\Omega^2\Delta_l + \sigma_\beta^2\frac{\Delta_l^3}{3} + \sigma_d^2\frac{\Delta_l^5}{20} & \sigma_\beta^2\frac{\Delta_l^2}{2} + \sigma_d^2\frac{\Delta_l^4}{8}\\ \sigma_\beta^2\frac{\Delta_l^2}{2} + \sigma_d^2\frac{\Delta_l^4}{8} & \sigma_\beta^2 + \sigma_d^2\frac{\Delta_l^3}{3}\end{bmatrix}. \tag{18}$$

A common maneuvering model for target motion [45] follows from the relationship between location, velocity and acceleration, and is given by

$$\begin{bmatrix}\mathbf{p}_1^{(l)}\\ \mathbf{v}_1^{(l)}\end{bmatrix} = \begin{bmatrix}\mathbf{I} & \Delta_l\mathbf{I}\\ \mathbf{0} & \mathbf{I}\end{bmatrix}\begin{bmatrix}\mathbf{p}_1^{(l-1)}\\ \mathbf{v}_1^{(l-1)}\end{bmatrix} + \underbrace{\begin{bmatrix}\frac{1}{2}\Delta_l^2\mathbf{a}^{(l-1)}\\ \Delta_l\mathbf{a}^{(l-1)}\end{bmatrix}}_{\triangleq\boldsymbol{\nu}_s^{(l-1)}}, \tag{19}$$

where $\mathbf{I}$ and $\mathbf{0}$ are the identity and zero matrices with appropriate sizes, and the control vector $\boldsymbol{\nu}_s^{(l)}$ describes the change of velocity during the observation interval Δ_l, which is related to the acceleration $\mathbf{a}^{(l)}$. When the receiver is moving with small variations in velocity, it is common to

model the acceleration as a continuous Wiener process with intensity $\sigma_{\mathbf{a}^{(l)}}$ [46], and hence we have $\mathbf{v}_s^{(l)} \sim \mathcal{N}\left(\mathbf{0}, \mathbf{Q}_s^{(l)}\right)$ where

$$\mathbf{Q}_s^{(l)} = \sigma^2_{\mathbf{a}^{(l)}} \begin{bmatrix} \frac{\Delta_l^5}{20} & 0 & 0 & \frac{\Delta_l^4}{8} & 0 & 0 \\ 0 & \frac{\Delta_l^5}{20} & 0 & 0 & \frac{\Delta_l^4}{8} & 0 \\ 0 & 0 & \frac{\Delta_l^5}{20} & 0 & 0 & \frac{\Delta_l^4}{8} \\ \frac{\Delta_l^4}{8} & 0 & 0 & \frac{\Delta_l^3}{3} & 0 & 0 \\ 0 & \frac{\Delta_l^4}{8} & 0 & 0 & \frac{\Delta_l^3}{3} & 0 \\ 0 & 0 & \frac{\Delta_l^4}{8} & 0 & 0 & \frac{\Delta_l^3}{3} \end{bmatrix}. \tag{20}$$

Combining (17) and (19), our receiver state model is given by

$$\underbrace{\begin{bmatrix} \mathbf{p}_1^{(l)} \\ \mathbf{v}_1^{(l)} \\ \theta^{(l)} \\ \alpha^{(l)} \end{bmatrix}}_{\mathbf{x}^{(l)}} = \underbrace{\begin{bmatrix} \mathbf{I} & \Delta_l \mathbf{I} & \mathbf{0} & \mathbf{0} \\ \mathbf{0} & \mathbf{I} & \mathbf{0} & \mathbf{0} \\ \mathbf{0} & \mathbf{0} & 1 & \Delta_l \\ \mathbf{0} & \mathbf{0} & 0 & 1 \end{bmatrix}}_{\triangleq \mathbf{H}_l} \underbrace{\begin{bmatrix} \mathbf{p}_1^{(l-1)} \\ \mathbf{v}_1^{(l-1)} \\ \theta^{(l-1)} \\ \alpha^{(l-1)} \end{bmatrix}}_{\mathbf{x}^{(l-1)}} + \boldsymbol{\nu}^{(l)}, \tag{21}$$

where $\boldsymbol{\nu}^{(l)} = [\boldsymbol{\nu}_c^{(l)}; \boldsymbol{\nu}_s^{(l)}] \sim \mathcal{N}(\mathbf{0}, \mathbf{Q}_l)$ is the process noise. We hence obtain

$$p\left(\mathbf{x}^{(l)} \middle| \mathbf{x}^{(l-1)}\right) \propto \exp\{-\frac{1}{2}(\mathbf{x}^{(l)} - \mathbf{H}_l \mathbf{x}^{(l-1)})^T \mathbf{Q}_l^{-1} (\mathbf{x}^{(l)} - \mathbf{H}_l \mathbf{x}^{(l-1)})\}. \tag{22}$$

The process covariance matrix $\mathbf{Q}_l$ is a block diagonal matrix consisting of $\mathbf{Q}_c^{(l)}$ and $\mathbf{Q}_s^{(l)}$.

Substituting $p\left(\mathbf{y}^{(l)} \middle| \mathbf{x}^{(l)}\right)$ and $p\left(\mathbf{x}^{(l)} \middle| \mathbf{x}^{(l-1)}\right)$ into (14) and (15), we can obtain the estimation of the state $\mathbf{x}^{(l)}$ in the l-th time slot as $\hat{\mathbf{x}}^{(l)} = \max_{\mathbf{x}^{(l)}} p\left(\mathbf{x}^{(l)} \middle| \mathbf{y}^{(1:l)}\right)$. The recursive relations (14) and (15) forms the basis for the optimal Bayesian solutions. When the integration cannot be obtained in closed form for general distributions, it can be solved by numerical methods such as particle filtering [42]. As we are assuming that all distributions are Gaussian, it leads to the well known Kalman filter (KF). However, since $p\left(\mathbf{y}^{(l)} \middle| \mathbf{x}^{(l)}\right)$ is associated with a nonlinear function $\mathbf{g}_b(\mathbf{x}^{(l)})$ (cf. (16)), to obtain a closed form solution, we first approximate $\mathbf{g}_b(\mathbf{x}^{(l)})$ by the Taylor series expansion using

$$\mathbf{G}_l = \nabla_{\mathbf{x}} \mathbf{g}_b(\mathbf{x})|_{\mathbf{x}=\mathbf{x}^{(l)}} = \begin{bmatrix} \mathbf{u}_{1,b}^{(l)} & \mathbf{w}_{1,b}^{(l)} \\ \mathbf{0} & \mathbf{u}_{1,b}^{(l)} \\ 1 & T_e^{(l)} \\ 0 & 1 \end{bmatrix}^T_{\mathbf{x}=\mathbf{x}^{(l)}}, \tag{23}$$

where $\mathbf{u}_{j,b}^{(l)}$ is the direction vector in (6), and $\mathbf{w}_{j,b}^{(l)}$ is the corresponding perpendicular direction vector defined as

$$\mathbf{w}_{j,b}^{(l)} = \frac{\mathbf{I} - \mathbf{u}_{j,b}^{(l)}(\mathbf{u}_{j,b}^{(l)})^T}{\left\|\mathbf{p}_j^{(l)} - \mathbf{p}_b^{(l)}\right\|}(\mathbf{v}_j^{(l)} - \mathbf{v}_b^{(l)}). \tag{24}$$

Substituting the approximation into (14) and (15) then leads to the extended Kalman filter (EKF) [47]. We have $p\left(\mathbf{x}^{(l)}\middle|\,\mathbf{y}^{(1:l-1)}\right) \approx \mathcal{N}\left(\mathbf{m}_{l|l-1}, \mathbf{P}_{l|l-1}\right)$ and $p\left(\mathbf{x}^{(l)}\middle|\,\mathbf{y}^{(1:l)}\right) \approx \mathcal{N}\left(\mathbf{m}_{l|l}, \mathbf{P}_{l|l}\right)$ with

$$\mathbf{m}_{l|l-1} = \mathbf{H}_l\mathbf{m}_{l-1|l-1}, \tag{25a}$$

$$\mathbf{P}_{l|l-1} = \mathbf{Q}_l + \mathbf{H}_l\mathbf{P}_{l-1|l-1}\mathbf{H}_l^T, \tag{25b}$$

$$\mathbf{P}_{l|l} = \mathbf{P}_{l|l-1} - \mathbf{K}_l\mathbf{G}_l\mathbf{P}_{l|l-1}, \tag{25c}$$

$$\mathbf{m}_{l|l} = \mathbf{m}_{l|l-1} + \mathbf{K}_l(\mathbf{y}^{(l)} - \mathbf{g}_b(\mathbf{m}_{l|l-1})), \tag{25d}$$

where $\mathbf{K}_l = \mathbf{P}_{l|l-1}\mathbf{G}_l^T(\mathbf{R}_l + \mathbf{G}_l\mathbf{P}_{l|l-1}\mathbf{G}_l^T)^{-1}$ represents the Kalman gain. We implement the sequential tracking and synchronization algorithm based on (25). The procedure starts with $\mathbf{m}_{0|0} = \bar{\mathbf{x}}_0$ and $\mathbf{P}_{0|0} = \bar{\mathbf{P}}_0$, where $\bar{\mathbf{x}}_0$ is the initial guess for parameters and $\bar{\mathbf{P}}_0$ describes our confidence in the initial guess. Every time the receiver R_1 obtains a new pair of TDOA and FDOA measurements, it updates $\mathbf{m}_{l|l}$ and $\mathbf{P}_{l|l}$ using (25), and obtains the estimate for the l-th observation period as $\hat{\mathbf{x}}^{(l)} = \mathbf{m}_{l|l}$.

Remark 2: If R_0 is not an anchor, one can generalize the above tracking algorithm to include $\{\mathbf{p}_0^{(l)}, \mathbf{v}_0^{(l)}\}$ as unknown parameters in each time slot. In particular, we will have $\mathbf{x}^{(l)} = [(\mathbf{p}_1^{(l)})^T, (\mathbf{v}_1^{(l)})^T, (\mathbf{p}_0^{(l)})^T, (\mathbf{v}_0^{(l)})^T, \theta^{(l)}, \alpha^{(l)}]^T$, and the dynamic model and the gradient matrix $\mathbf{G}_l$ can be updated accordingly. With sufficient measurements, the states of both receivers can be estimated simultaneously, which is similar to [17]. However, we have found that the estimation performance is sensitive to how accurately we know the beacons' positions and velocities, where any errors translate to systematic biases in the receivers' location and velocity estimates. In our empirical studies, we have used Iridium satellites as the beacons, and computed their positions and velocities using the SGP4 model. Studies have shown that the SGP4 model can produce position errors up to 10 km [25], which can lead to meaningless location estimates for the receivers. Therefore, in this paper, we have assumed that the receiver R_0 acts as an anchor that provides a reference point to the receiver R_1.

C. CRB discussion

In this section, we derive the CRB for joint localization and synchronization using SOOPs by considering the parameters of interest to be $\bar{\mathbf{x}}^{(l)} = \mathbb{E}[\mathbf{x}^{(l)}]$, for $l \geq 1$. Our derivation is based on the received sample sequences $\{\tilde{\mathbf{r}}_{j,b}^{(l)}\}_{j=0,1}$, which implies that our derived CRB applies to all estimation methods and measurement metrics [17], unlike [34] in which the CRB is based on the TDOA/FDOA measurements. For simplicity, we consider a sequential estimation where only one beacon b is available during each observation period. Our analysis can be easily extended to the case where multiple beacons are available at each observation period.

In the l-th observation period, from (21), we have $\mathbf{x}^{(l)} = \bar{\mathbf{x}}^{(l)} + \boldsymbol{\nu}^{(l)}$, where $\boldsymbol{\nu}^{(l)} \sim \mathcal{N}(\mathbf{0}, \mathbf{Q}_l)$, and $\bar{\mathbf{x}}^{(l)} = \mathbf{H}_l \bar{\mathbf{x}}^{(l-1)}$. In the non-Bayesian framework, we aim to estimate $\bar{\mathbf{x}}^{(l)}$, and in the L-th period the likelihood function for $\bar{\mathbf{x}}^{(L)}$ is given by

$$p\left(\{\tilde{\mathbf{r}}_{j,b}^{(l)}\}_{l=1}^{L}; \bar{\mathbf{x}}^{(L)}\right) = \prod_{l=1}^{L} p(\tilde{\mathbf{r}}_{j,b}^{(l)}; \bar{\mathbf{x}}^{(l)}),$$

where $p(\bullet; \bar{\mathbf{x}}^{(l)})$ represents the likelihood function with $\bar{\mathbf{x}}^{(l)}$ as a parameter, and for $l < L$,

$$\bar{\mathbf{x}}^{(l)} = \prod_{t=l+1}^{L} (\mathbf{H}_t)^{-1} \cdot \bar{\mathbf{x}}^{(L)}.$$

The Fisher information matrix (FIM) for estimating $\mathbf{x}^{(L)}$ can be shown to be [47],

$$\mathbf{F}_{\bar{\mathbf{x}}}(L) = \sum_{l=1}^{L} \sum_{j=0,1} \mathcal{R}\mathrm{e}\left\{ \left(\frac{\partial \mathbf{r}_{j,b}^{(l)}}{\partial \bar{\mathbf{x}}^{(L)}} \right) \mathbf{C}_j^{-1} \left(\frac{\partial \mathbf{r}_{j,b}^{(l)}}{\partial \bar{\mathbf{x}}^{(L)}} \right)^H \right\} + \sum_{l=1}^{L} \left[\left(\frac{\partial \bar{\mathbf{x}}^{(l)}}{\partial \bar{\mathbf{x}}^{(L)}} \right) \mathbf{Q}_l^{-1} \left(\frac{\partial \bar{\mathbf{x}}^{(l)}}{\partial \bar{\mathbf{x}}^{(L)}} \right)^T \right], \quad (26)$$

where $(\cdot)^H$ denotes the conjugate transpose. In (26), the second term captures the accumulated effect of the model error due to unknown acceleration and clock drifting rate. The first term on the other hand captures the effect of other factors like measurement noise and beacon geometry, when the receiver state model is noiseless. From the differentiation chain rule, we have

$$\frac{\partial \mathbf{r}_{j,b}^{(l)}}{\partial \bar{\mathbf{x}}^{(L)}} = \frac{\partial \bar{\mathbf{x}}^{(l)}}{\partial \bar{\mathbf{x}}^{(L)}} \cdot \frac{\partial \mathbf{r}_{j,b}^{(l)}}{\partial \bar{\mathbf{x}}^{(l)}},$$
$$\frac{\partial \bar{\mathbf{x}}^{(l)}}{\partial \bar{\mathbf{x}}^{(L)}} = \left[\prod_{t=l+1}^{L} (\mathbf{H}_t)^{-1} \right]^T,$$

where $\mathbf{r}_{j,b}^{(l)}$ is given in (10) and $\mathbf{H}_t$ is given in (21). We can then rewrite (26) as

$$\mathbf{F}_{\bar{\mathbf{x}}}(L) = \sum_{l=1}^{L} \left(\frac{\partial \bar{\mathbf{x}}^{(l)}}{\partial \bar{\mathbf{x}}^{(L)}} \right) \left[\tilde{\mathbf{F}}_{\bar{\mathbf{x}}}(l) + \mathbf{Q}_l^{-1} \right] \left(\frac{\partial \bar{\mathbf{x}}^{(l)}}{\partial \bar{\mathbf{x}}^{(L)}} \right)^T, \quad (27)$$

with

$$\tilde{\mathbf{F}}_{\bar{\mathbf{x}}}(l) = \mathcal{R}\mathrm{e}\left\{\sum_{j=0,1}\left(\frac{\partial \mathbf{r}_{j,b}^{(l)}}{\partial \bar{\mathbf{x}}^{(l)}}\right)\mathbf{C}_j^{-1}\left(\frac{\partial \mathbf{r}_{j,b}^{(l)}}{\partial \bar{\mathbf{x}}^{(l)}}\right)^H\right\}. \tag{28}$$

Note that $\tilde{\mathbf{F}}_{\bar{\mathbf{x}}}(l)$ represents the instantaneous FIM at the l-th time slot. We further map the parameter vector $\bar{\mathbf{x}}^{(l)}$ into another parameter vector $\bar{\mathbf{y}}^{(l)} = [\bar{\tau}_b^{(l)}, \bar{\xi}_b^{(l)}]$ with elements corresponding to the noise-free TDOA and FDOA measurements in (13). Substituting $\partial\bar{\mathbf{y}}^{(l)}/\partial\bar{\mathbf{x}}^{(l)} = \mathbf{G}_l$ in (23) and again utilizing the chain rule, we have

$$\tilde{\mathbf{F}}_{\bar{\mathbf{x}}}(l) = \mathbf{G}_l\tilde{\mathbf{F}}_{\bar{\mathbf{y}}}(l)\mathbf{G}_l^T, \tag{29}$$

where $\tilde{\mathbf{F}}_{\bar{\mathbf{y}}}(l)$ represents the instantaneous FIM for estimating $\bar{\tau}_b^{(l)}$ and $\bar{\xi}_b^{(l)}$ using the received sequences $\{\tilde{\mathbf{r}}_{j,b}^{(l)}\}_{j=1,2}$. Following a similar procedure in [17], it can be shown that

$$\tilde{\mathbf{F}}_{\bar{\mathbf{y}}}(l) \approx 8\pi^2\mathsf{SNR}_b\begin{bmatrix}\mathsf{W}_b^2\sum_j\beta_j & 0\\ 0 & \mathsf{T}_b^2\sum_j\beta_j\end{bmatrix}, \tag{30}$$

where SNR_b is the SNR for the received signal, and we define the root-mean-square (rms) bandwidth W_b, and the rms integration time T_b for the transmit signal $s_b(t)$ as follows [37], [48],

$$\mathsf{W}_b = \left[\frac{\int |fS_b(f)|^2\mathrm{d}f}{\int |S_b(f)|^2\mathrm{d}f}\right]^{\frac{1}{2}},$$

$$\mathsf{T}_b = \left[\frac{\int |ts_b(t)|^2\mathrm{d}t}{\int |s_b(t)|^2\mathrm{d}t}\right]^{\frac{1}{2}}.$$

with $S_b(f)$ as the Fourier transform of $s_b(t)$. The FIM $\tilde{\mathbf{F}}_{\bar{\mathbf{y}}}^{(l)}$ characterizes the estimation accuracy for TDOA/FDOA measurements, which is completely determined by signal properties like SNR, signal bandwidth, and integration time.

Finally, a closed-form expression for the FIM for estimating $\bar{\mathbf{x}}^{(L)}$ is given by

$$\mathbf{F}_{\bar{\mathbf{x}}}(L) = \sum_{l=1}^{L}\left[\prod_{t=l+1}^{L}(\mathbf{H}_t)^{-1}\right]^T\left[\mathbf{G}_l\tilde{\mathbf{F}}_{\bar{\mathbf{y}}}(l)\mathbf{G}_l^T + \mathbf{Q}_l^{-1}\right]\left[\prod_{t=l+1}^{L}(\mathbf{H}_t)^{-1}\right]. \tag{31}$$

The estimation accuracy for $\bar{\mathbf{x}}^{(l)}$ thus depends on the measurement accuracy characterized by $\tilde{\mathbf{F}}_{\bar{\mathbf{y}}}^{(l)}$, the state dynamics characterized by $\mathbf{G}_l$, and the observation schedule characterized by $\mathbf{H}_t$. The matrix $\mathbf{G}_l$, consisting of direction vectors $\mathbf{u}_{1,b}^{(l)}$ and $\mathbf{w}_{1,b}^{(l)}$, depends on relative positions and velocities of the receivers w.r.t. the beacon at time $t^{(l)}$. It can be shown that $\mathbf{G}_l\tilde{\mathbf{F}}_{\bar{\mathbf{y}}}(l)\mathbf{G}_l^T$ is always rank deficient due to the fact that only one beacon is available at each time. A feasible solution can

hence be obtained from the sequential estimator only after multiple observation periods in order to accumulate a set of spanning vectors.

Furthermore, it can be shown that $\mathbf{G}_l\tilde{\mathbf{F}}_{\bar{\mathbf{y}}}(l)\mathbf{G}_l^T$ is positive semi-definite for all l and $\mathbf{F}_{\bar{\mathbf{x}}}(L) = (\mathbf{H}_L^{-1})^T\mathbf{F}_{\bar{\mathbf{x}}}(L-1)\mathbf{H}_L^{-1} + \mathbf{G}_L\tilde{\mathbf{F}}_{\bar{\mathbf{y}}}(L)\mathbf{G}_L^T + \mathbf{Q}_L^{-1}$. If the observation is so frequent that the observation period approaches zero, i.e., $\Delta_l \to 0$, we have $\mathbf{H}_l^{-1} = \mathbf{I}$ for all l and $\mathbf{F}_{\bar{\mathbf{x}}}(L) - \mathbf{F}_{\bar{\mathbf{x}}}(L-1) \geq 0$. It implies that the estimation performance improves as more observations are available, and it holds true even when the target is maneuvering, since every movement of the target was captured in the observation and can be tracked in time. However, this is not necessarily true when additional errors are accumulated over a long time due to the dynamic model inaccuracy.

To further investigate the effect of observation frequency, we calculate the trace of $\mathbf{F}_{\bar{\mathbf{x}}}(L)$ under simplifying assumptions. Let the diagonal elements of $\tilde{\mathbf{F}}_{\bar{\mathbf{y}}}(l)$ be a_l and b_l. Suppose that the clock offset and clock skew are relatively stable with $\sigma_\Omega = 0$ and $\sigma_\beta = 0$, and the diffusion of clock drifting is characterized by σ_d, we let $c_l = 48/\sigma^2_{\mathbf{a}^{(l)}} + 16/\sigma_d^2$. It can be shown that

$$\begin{aligned}\mathrm{Tr}\left\{\mathbf{F}_{\bar{\mathbf{x}}}(L)\right\} = &\sum_{l=1}^{L-1}\left[\Lambda_l^2(2a_l+b_l) + (2a_l+3b_l)\right] + \sum_{l=1}^{L-1} c_l\left(20\Lambda_l^2\Delta_l^{-5} - 15\Lambda_l\Delta_l^{-4} + 20\Delta_l^{-5} + 3\Delta_l^{-3}\right)\\ &+ \mathrm{Tr}\left\{\mathbf{G}_L\tilde{\mathbf{F}}_{\bar{\mathbf{y}}}(L)\mathbf{G}_L^T + \mathbf{Q}_L^{-1}\right\},\end{aligned} \tag{32}$$

with $\Lambda_l = -\sum_{t=l+1}^{L}\Delta_l$. Assuming the observation is taken periodically with $\Delta_l = \Delta$, it can be shown from (32) that $\mathrm{Tr}\left\{\mathbf{F}_{\bar{\mathbf{x}}}(L)\right\}$ without the terms independent of Δ is given by

$$\sum_{l=1}^{L-1}(2a_{L-l}+b_{L-l})l^2\Delta^2 + \sum_{l=1}^{L-1} c_{L-l}\left[\left(20l^2+15l+3\right)\Delta^{-3} + 20\Delta^{-5}\right]. \tag{33}$$

The first sum in (33) represents the information from measurements, and the second sum represents the information from the dynamic state update. When the inter-observation duration Δ is fixed, both sums in (33) increase with the number of observations L. However, when we are allowed to take only a fixed L number of observations, the inter-observation interval Δ should be carefully chosen to balance the contributions from the measurement and the state dynamics. Specifically, the first sum in (33) increases with the value of Δ because a larger Δ provides a longer integration time and hence results in measurements with better accuracy. However, the second sum decreases with the value of Δ, as less frequent observations result in error accumulation in the dynamic state model. By taking the first derivative of (33) w.r.t. Δ and setting to zero, the optimal Δ can be found numerically by solving $\psi_1\Delta^7 - \psi_2\Delta^2 - \psi_3 = 0$, where $\psi_1 = 2\sum_{l=1}^{L-1}(2a_{L-l}+b_{L-l})l^2$, $\psi_2 = 3\sum_{l=1}^{L-1} c_{L-l}\left(20l^2+15l+3\right)$, $\psi_3 = 100\sum_{l=1}^{L-1} c_{L-l}$.

IV. Empirical Experiments and Simulations

In order to evaluate the proposed measurement model (13) for TDOA and FDOA estimation and the proposed algorithm (25), we have conducted extensive experiments using real life data. In this section, we present a set of experimental and simulation results to verify the correctness of our models and performance of our proposed algorithm.

A. Experiment setup

The Iridium satellites are used as SOOP beacons due to their wide coverage and easy availability. Specifically, we make use of the broadcast signal in the Iridium ring alert channel whose downlink frequency is fixed at 1626.270833 MHz. The ring alert signal is broadcast by all Iridium satellites periodically. A drawback is that the ring alert signal is broadcast only every 4.32 second, which is a relatively long period for tracking a fast maneuvering receiver. More signals from the Iridium satellites, such as those from the downlink traffic channels, message channel, and synchronization channel, can be used to achieve better performance. In this experiment, we focused only on the ring alert signal as a proof of concept.

The receiver used is a software-defined radio (SDR) testbed. In our experiments, we used the USRP-N210 SDR with WBX daughterboard [49]. The USRP is connected to and controlled by a standard PC with large and fast storage space. Other components in one receiver set include one Iridium antenna, one low noise amplifier (LNA) ZHL-1217MLN, one standard DC power supply, and one portable battery. A complete receiver is shown in Figure 2.

Our experiment was conducted in Singapore with three sets of receivers. Two receivers, A and B, were static. Receiver A was placed on the rooftop of a building on the Nanyang Technological University (NTU) campus on the western side of Singapore, while receiver B was located near Changi Airport on the eastern side of Singapore. These two receivers are at a distance of approximately 36 km apart. Both receivers A and B have open sky views so that they can receive Iridium signals with relatively high SNR. The third receiver C is placed in a car which moved from Changi Airport to NTU. The positions of receivers A and B, and the trajectory of receiver C are shown in Figure 3. A separate GPS receiver is placed in the car together with receiver C so that the GPS trajectory of receiver C can be used as a benchmark for comparison.

All three USRPs in the receivers used free-running local oscillators without any form of synchronization between them. The USRPs are set to receive at the frequency 1626.27 MHz with a sampling rate of 10 MHz. To guarantee that all receivers see the same satellite, as stated in

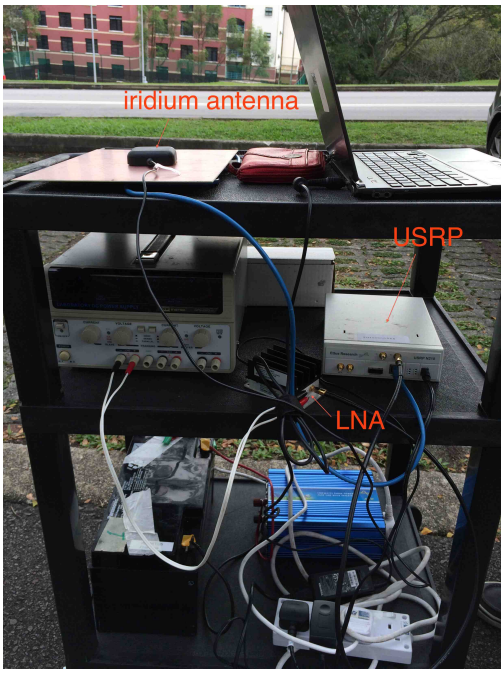

Fig. 2. A receiver used in our experiment.

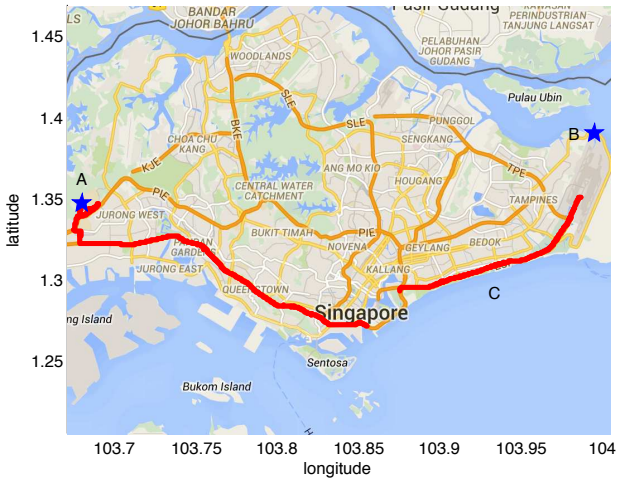

Fig. 3. Locations of receivers A and B, and trajectory of receiver C, where the discontinuity in the trajectory is due to driving in a tunnel.

Assumption 1(iii), we pre-calibrated the laptop clock before the experiment to an accuracy of one second, and we use the laptop time to initiate the recording at each receiver.

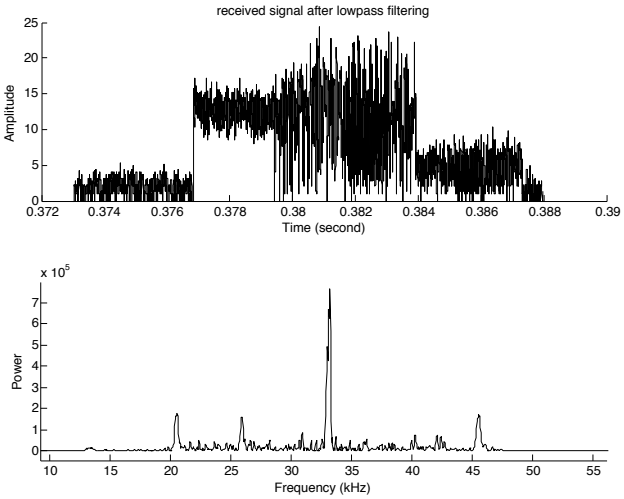

Fig. 4. One example baseband packet detected at receiver A.

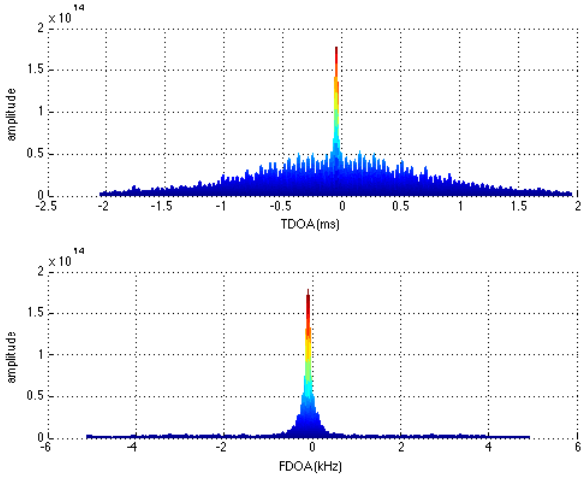

Fig. 5. The amplitude of the complex cross-correlation function between two packets, one from receiver A, another from receiver B in the same observation time slot.

B. Validating measurement model (13)

To verify the measurement model (13), we collected data over a continuous period lasting about 48 minutes. In total 8 Iridium satellites were observed. For any two receivers, their received signals are processed off-line in three steps:

1) Packet detection: a typical ring alert burst lasts for 7 ms, and its average power is much higher than the noise floor. We divide the signal segment into intervals of 15 ms. Within each interval,

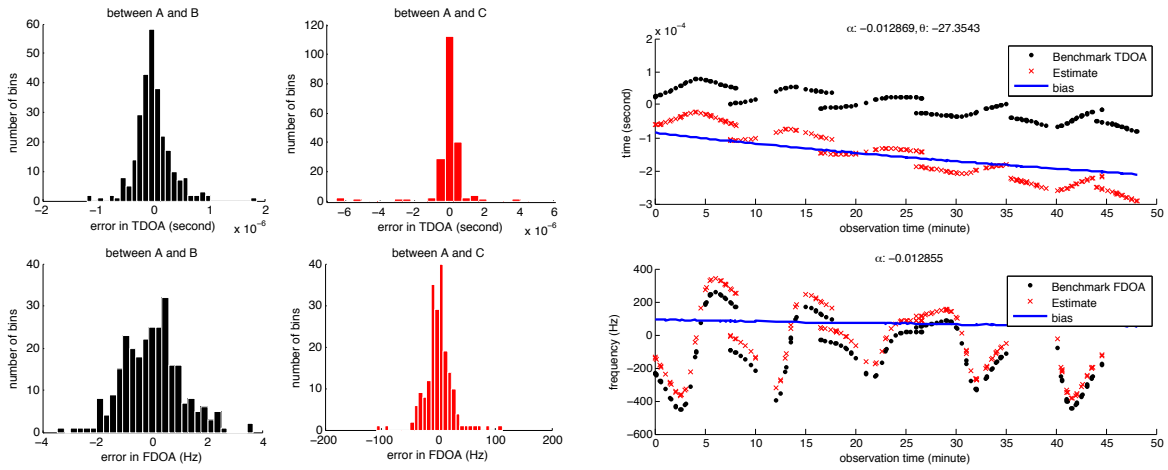

(a) Histogram for TDOA and FDOA measurement errors.

(b) TDOA and FDOA benchmark and empirical values for the receiver pair A and B.

Fig. 6. TDOA and FDOA measurements between two receivers; bias is calculated by subtracting benchmark value from the estimation.

we compute the power in a sliding window of length 7ms, and we declare a packet exists in this interval if the power in the window is twice higher than the total power in the interval.

2) Lowpass filtering: a lowpass filter is used to remove signals from other bands. Since the speed of an Iridium satellite is 7.4km/s, the maximum Doppler shift induced in the received signal is 40 KHz. We therefore apply a 100 KHz bandwidth lowpass filter to the baseband signal. An example of ring alert signal packet after lowpass filtering is shown in Figure 4. Its time domain signal shows a clear pilot tone signal in the beginning followed by a DE-QPSK modulated data sequence.
3) TDOA and FDOA estimation: with packets detected at both receivers, their perspective TDOA and FDOA can be obtained by maximizing the amplitude of the complex ambiguity function of the corresponding packets [37]. An example of the complex ambiguity function is shown in Figure 5, where the TDOA and FDOA estimates correspond to the time and frequency value of the maximal point.

To determine the biases in the empirical TDOA and FDOA values we have obtained in our experiments, we obtain the positions and velocities of the receivers using GPS, and compute the positions and velocities of the Iridium satellites using the SGP4 model [24], [50]. The benchmark TDOA and FDOA values are then computed using these values. The histograms for TDOA and FDOA measurement errors are plotted in Figure 6(a) for those between receivers A and B as well

as those between receivers A and C. The statistics are different for the two receiver pairs due to differences in their environments, and estimation accuracies.

To validate the measurement model (13), we take the TDOA and FDOA measurements between receiver A and B as an illustrative example. In total, we detected 286 packets, which give rise to 286 pairs of TDOA and FDOA estimates as shown in Figure 6(b). The bias is computed by subtracting the benchmark TDOA and FDOA values from the empirical values we have estimated. It can be seen that the biases in both TDOA and FDOA are linear, which show a good match with our measurement model (13). Using linear regression over the bias values, we obtain $\alpha = -0.012869$ using the TDOA biases and $\alpha = -0.012855$ using the FDOA biases. The difference between the estimated values for α is at the order of 10^{-5} and is due to the approximation in (12) as well as estimation errors.

C. Experiment results for localizing static receiver

With the estimated TDOA and FDOA, we apply our proposed algorithm in (25) to jointly estimate the receiver B's location and its clock parameters, where receiver A is the anchor. The estimation results are shown in Figure 7. One important user-defined factor in the proposed algorithm is the value of the covariance matrix $\mathbf{R}_l$ for measurement noise and $\mathbf{Q}_l$ for state dynamics. In our implementation, we set $\mathbf{R}_l$ to be a diagonal matrix with its component standard deviation values following from the CRB values in (30). We set $\sigma_\Omega = 10^{-10}$, $\sigma_\beta = 10^{-9}$, and $\sigma_d = 10^{-8}$ for $\mathbf{Q}_c^{(l)}$ in (18) according to the datasheet for the oscillator used in the USRP-N210 [49]. Since the receiver B is static, it has no acceleration, therefore we let $\sigma_{\mathbf{a}} = 10^{-10}$ for $\mathbf{Q}_s^{(l)}$ in (20).

Figure 7(a) shows the results for tracking the relative clock parameters between the two receivers A and B using our proposed algorithm in (25). In the left column, we show the empirical relative clock parameters found by subtracting the benchmark TDOA and FDOA values from the empirical values we have estimated, and the tracked relative clock parameters $\alpha^{(l)}$ and $\theta^{(l)}$ over a period of 48 minutes. It can be seen that our algorithm can track the relative clock parameters closely. In the lower-left subfigure, the empirical clock skew is at the order of 10ns/s, which conforms to the 0.01ppm specified in the USRP-N210 datasheet [49]. As the clock skew increases slightly over time, it results in a second order behavior in the clock offset drifting, as shown in the upper-left subfigure. The more detailed results and its comparison with CRB are shown in Figure 7(b), where the estimation error for clock parameters are calculated by subtracting the tracked relative clock parameters from their empirical values.

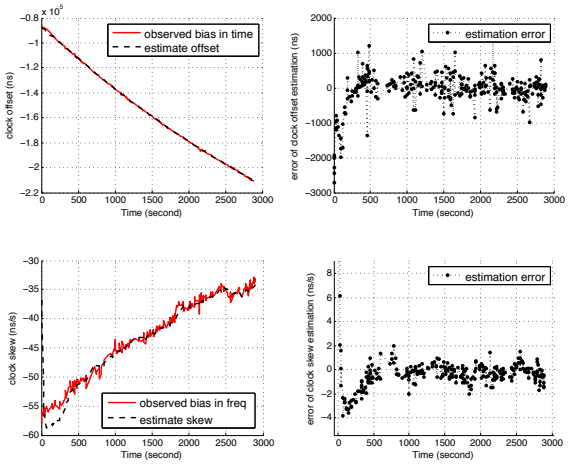

(a) Tracking relative clock parameters.

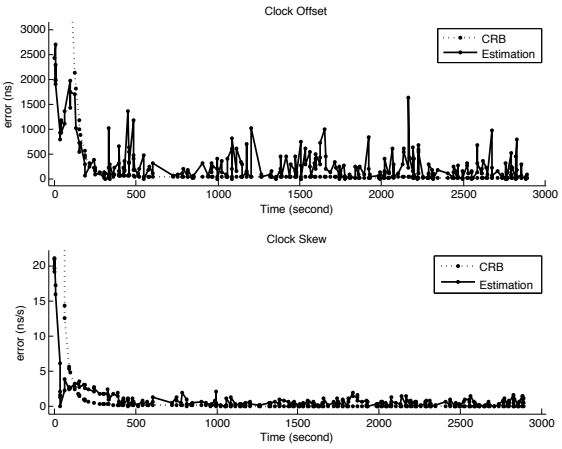

(b) Errors for estimating the clock parameters.

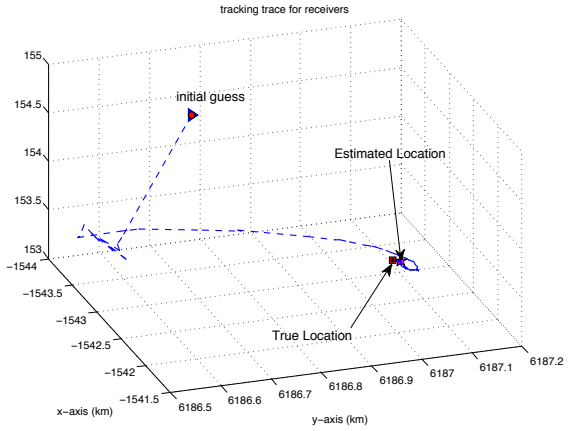

(c) Trace for estimating the receiver location.

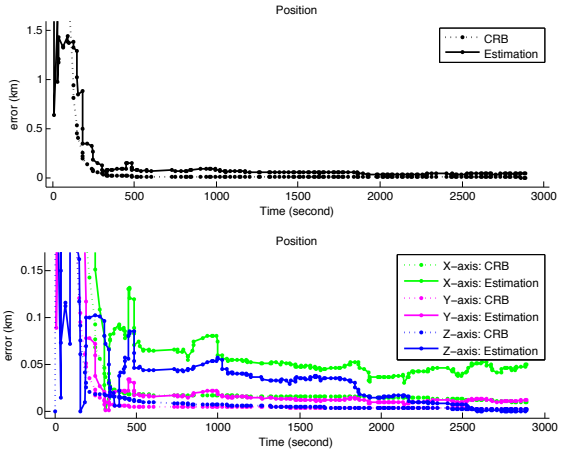

(d) Errors for estimating the receiver location.

Fig. 7. The proposed algorithm for jointly estimating static receiver B's location and relative clock parameters.

In Figure 7(c), we show the tracked locations of receiver B over time. The initial guess is a random point 5 km away from the true location receiver B. It can be seen that as more Iridium satellite signals are observed, our estimates converge to the true location. Our algorithm achieves an estimation error smaller than 50 meters within 5 minutes. The more detailed results are shown in Figure 7(d), where we have used the CRB calculated by (26) as a benchmark (in dashed line). The estimation error for positions are calculated w.r.t. the true location, and that for the relative clock parameters are calculated w.r.t. the empirical relative clock parameters. For the location estimation, it can be seen from the lower subfigure that the estimation error is dominated by the error from the x-axis, which corresponds to the direction from Earth to the Iridium satellites, while the errors

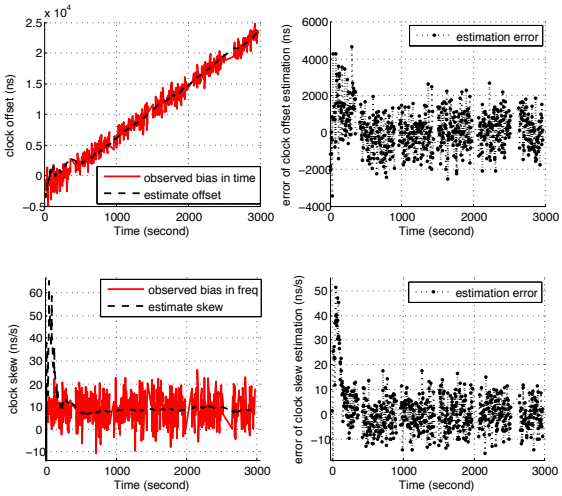

(a) Performance for tracking relative clock parameters in one simulation run.

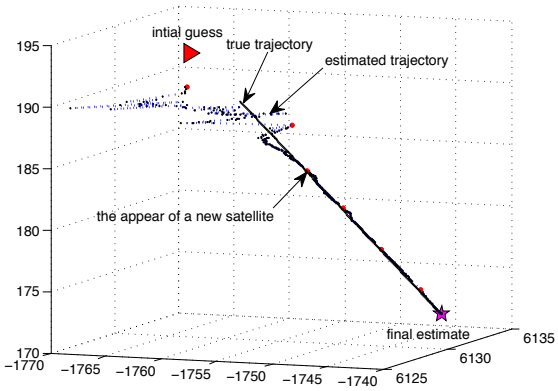

(b) Trace for tracking the receiver's movement in one simulation run.

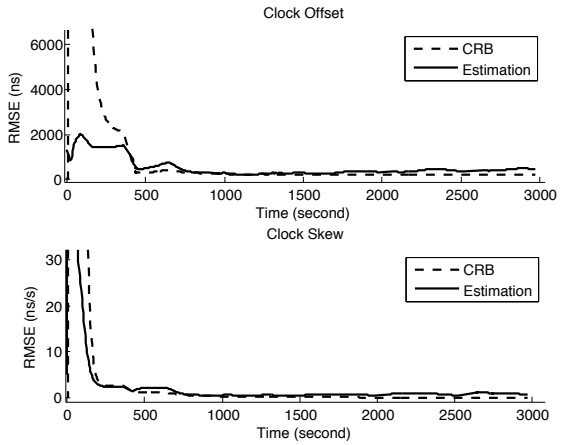

(c) RMSE for tracking the receiver clock parameters

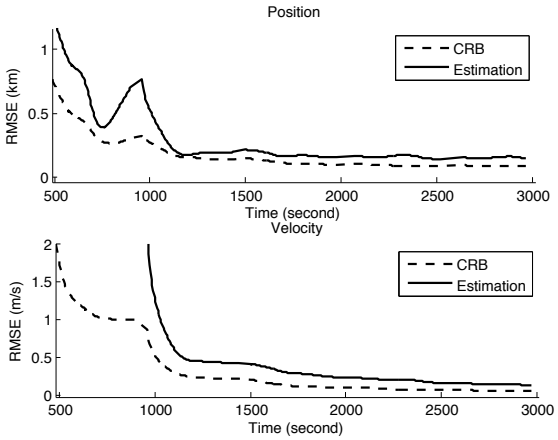

(d) RMSE for tracking the receiver state

Fig. 8. Jointly tracking a receiver moving with constant velocity.

from the other two axises, y and z, are close to the CRB. This is due to the fact that all satellite beacons are overhead and form an unfavorable geometry for localizing receiver B in the x-axis, similar to the poor altitude resolution commonly seen in GPS navigation. Assuming the altitude of the receiver is known exactly, the average error for the estimation from $t = 600.5$ seconds to the end of the experiment $t = 2887.8$ seconds is 26.7 meters, while the average error for the case without altitude information is 64.8 meters.

D. Simulation results for tracking receiver with constant velocity

In this subsection, to demonstrate the performance of our proposed algorithm (25) for tracking a mobile receiver moving with constant velocity, we conduct simulations instead of experiments because of the difficulty of finding a sufficiently long and straight path in Singapore to conduct our experiments. In the next subsection, we show experimental results for a receiver moving with non-constant velocity. In our simulations, the receiver moves with a constant velocity of [5; 1; -6] m/s and zero acceleration. The receiver A is used as an anchor. The clock offset and skew are simulated as a Gaussian random variables with zero mean and standard deviation 10^{-8}, and their values follow the linear model in (17). The measurement noises are simulated as Gaussian random variables with zero mean and standard deviation 10^{-6} second for TDOA and 10 Hz for FDOA, which conform to the statistics of measurement noise in the empirical experiment in Sections IV-B and IV-C. The results for tracking the receiver states are shown in Figure 8, and the root-mean squared error (RMSE) are averaged over 1000 simulation runs. It can be seen that our proposed algorithm achieves satisfactory performance in jointly tracking the receiver location, velocity and its relative clock parameters. Specifically, the estimated relative clock skews $\alpha^{(l)}$ and clock offsets $\theta^{(l)}$ have zero mean errors, as shown in Figure 8(a). The receiver position is tracked with RMSE smaller than 100 m and its velocity tracked with RMSE smaller than 0.1 m/s. In Figure 8(c) and Figure 8(d), it shows that the performance for estimating clocks parameters, position, and velocity all approach their respective CRBs.

E. Experiment results for tracking maneuvering receiver

With TDOA and FDOA measurements between receiver A and C, we apply the proposed algorithm (25) to track receiver C w.r.t. receiver A. The results are shown in Figure 9. As observed in our experiment results, one key factor that affects the tracking performance is the correctness of the dynamic state model (21). For the static case in Section IV-C, the dynamic model (19) is simplified with $\mathbf{v}^{(l)} = \mathbf{0}$ and the acceleration acts like a white noise term with zero mean and standard deviation 10^{-10} km/s^2. When the receiver is moving with constant velocity as in Section IV-D, the dynamic model (19) still provides a good match with a white-noise-like acceleration. However, when the receiver is maneuvering, e.g., taking turns and changing directions like receiver C in our experiment, the dynamic model (19) cannot accurately characterize the movement of the receiver especially when it is taking a sharp turn. In addition, as discussed in Section IV-A, the infrequent ring alert bursts limit the number of measurements. Therefore, the estimation error

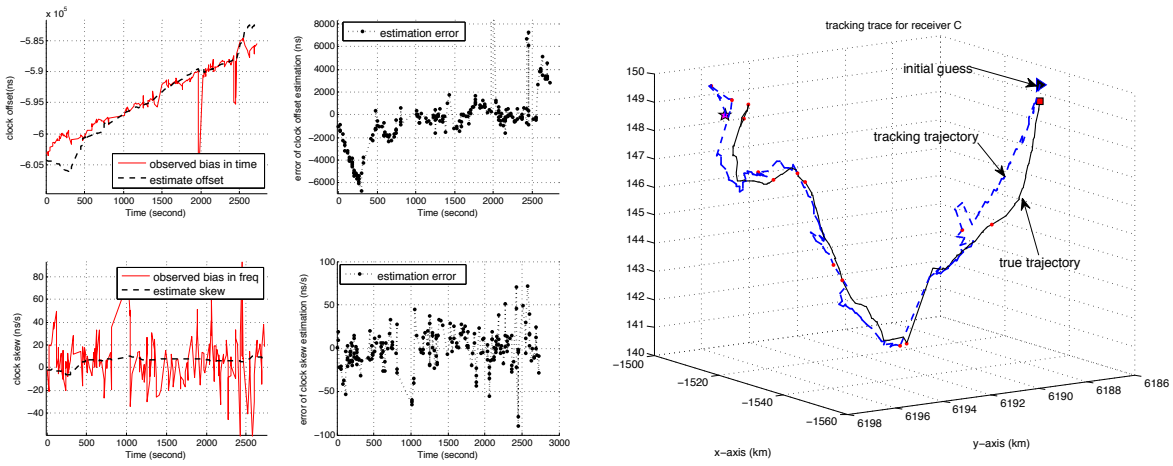

(a) Tracking clock drifting parameters

(b) Tracking the receiver state

Fig. 9. The proposed algorithm for tracking the maneuvering receiver C.

accumulated from previous time slots cannot be corrected timely during the maneuverings, resulting in larger errors, as is clear from parts of the trace in Figure 9(b). However, if the receiver C is moving with relatively constant velocity, the algorithm is able to reduce its tracking errors, as seen in the middle part of the trajectory in Figure 9(b).

V. CONCLUSION

In this paper, we have investigated the problem of joint localization and synchronization using SOOP in GPS-denied environments. We assume two receivers have free-running oscillators, and we assume all beacons are unsynchronized with unknown clock offsets. Considering a general scenario where an anchor exists to share the received signal and the state information with the target receiver, we analysed the biases introduced by asynchronous clocks in the received signal, we derived a closed-form expression for TDOA and FDOA measurements, and we proposed a sequential algorithm to jointly estimate the receiver state and its clock parameters. Receivers were implemented on SDR testbed, and field experiments were conducted with Iridium satellites as SOOP beacons. Experimental results showed that our measurement model for TDOA and FDOA correctly describes the relationship between biases and clock parameters, and our proposed algorithm can track the receiver state and clock parameters with good accuracy when the dynamic model correctly characterize the change of the receiver state.

REFERENCES

[1] S.-H. Fang, J.-C. Chen, H.-R. Huang, and T.-N. Lin, "Is FM a RF-based positioning solution in a metropolitan-scale environment? A probabilistic approach with radio measurements analysis," *IEEE Trans. Broadcast.*, vol. 55, no. 3, pp. 577–588, 2009.

[2] M. Rabinowitz and J. Spilker, J. J., "A new positioning system using television synchronization signals," *IEEE Trans. Broadcast.*, vol. 51, no. 1, pp. 51–61, 2005.

[3] D. Serant, P. Thevenon, M.-L. Boucheret, O. Julien, C. Macabiau, S. Corazza, M. Dervin, and L. Ries, "Development and validation of an OFDM/DVB-T sensor for positioning," in *Proc. IEEE/ION Position Location and Navigation Symp. (PLANS)*, 2010, pp. 988–1001.

[4] H. Namie, K. Nishikawa, K. Sasano, C. Fan, and A. Yasuda, "Development of network-based RTK-GPS positioning system using FKP via a TV broadcast in Japan," *IEEE Trans. Broadcast.*, vol. 54, no. 1, pp. 106–111, 2008.

[5] D.-B. Lin and R.-T. Juang, "Mobile location estimation based on differences of signal attenuations for GSM systems," *IEEE Trans. Veh. Technol.*, vol. 54, no. 4, pp. 1447–1454, 2005.

[6] Z. R. Zaidi and B. L. Mark, "Real-time mobility tracking algorithms for cellular networks based on Kalman filtering," *IEEE Trans. Mobile Comput.*, vol. 4, no. 2, pp. 195–208, 2005.

[7] M. Bshara, U. Orguner, F. Gustafsson, and L. Van Biesen, "Robust tracking in cellular networks using HMM filters and cell-ID measurements," *IEEE Trans. Veh. Technol.*, vol. 60, no. 3, pp. 1016–1024, 2011.

[8] H. Lemelson, M. B. Kjaergaard, R. Hansen, and T. King, "Error estimation for indoor 802.11 location fingerprinting," in *Proc. Int. Symposium on Location and Context Awareness*, ser. LoCA '09. Berlin, Heidelberg: Springer-Verlag, 2009, pp. 138–155.

[9] H. Lim, L.-C. Kung, J. C. Hou, and H. Luo, "Zero-configuration indoor localization over IEEE 802.11 wireless infrastructure," *Wirel. Netw.*, vol. 16, no. 2, pp. 405–420, Feb. 2010. [Online]. Available: http://dx.doi.org/10.1007/s11276-008-0140-3

[10] Y.-S. Chiou, C.-L. Wang, and S.-C. Yeh, "An adaptive location estimator using tracking algorithms for indoor WLANs," *Wirel. Netw.*, vol. 16, no. 7, pp. 1987–2012, Oct. 2010.

[11] R. Kaune, C. Steffes, S. Rau, W. Konle, and J. Pagel, "Wide area multilateration using ads-b transponder signals," in *Int. Conf. on Information Fusion*, July 2012, pp. 727–734.

[12] Iridium satellite phone communications. [Online]. Available: https://www.iridium.com/default.aspx

[13] K. A. Fisher, *The Navigation Potential of Signals of Opportunity-based Time Difference of Arrival Measurements*. Air Force Institude of Technologty, 2005.

[14] N. Bulusu, J. Heidemann, and D. Estrin, "GPS-less low-cost outdoor localization for very small devices," *IEEE Personal Commun.*, vol. 7, no. 5, pp. 28–34, 2000.

[15] W. P. Tay, J. N. Tsitsiklis, and M. Z. Win, "Bayesian detection in bounded height tree networks," *IEEE Trans. Signal Process.*, vol. 57, no. 10, pp. 4042–4051, Oct 2009.

[16] W. P. Tay, "The value of feedback in decentralized detection," *IEEE Trans. Inf. Theory*, vol. 58, no. 12, pp. 7226–7239, Dec. 2012.

[17] M. Leng, W. P. Tay, C. M. S. See, and S. G. Razul, "Modified CRLB for cooperative geolocation of two devices using signals of opportunity," *IEEE Trans. Wireless Commun.*, vol. 13, no. 7, pp. 3636–3649, 2014.

[18] M. Leng and W. P. Tay, "Fundamental limits of self-localization for cooperative robotic platforms using signals of opportunity," in *Cooperative Robots and Sensor Networks*. New York, NY: Springer, 2015.

[19] W. Xu, F. Quitin, M. Leng, W. P. Tay, and S. G. Razul, "Distributed localization of a RF target in NLOS environments," *IEEE J. Sel. Areas Commun.*, 2015, in press.

[20] J. Mick. (2011, December) Iran: Yes, we hacked the u.s.'s drone, and here's how we did it. [Online]. Available: http://www.dailytech.com/Iran+Yes+We+Hacked+the+USs+Drone+and+Heres+How+We+Did+It/article23533.htm

[21] M. Robinson and R. Ghrist, "Topological localization via signals of opportunity," *IEEE Trans. Signal Process.*, vol. 60, no. 5, pp. 2362–2373, 2012.

[22] N. Patwari, J. N. Ash, S. Kyperountas, A. O. H. III, R. L. Moses, and N. S. Correal, "Locating the nodes: cooperative localization in wireless sensor networks," *IEEE Signal Process. Mag.*, vol. 22, no. 4, pp. 54–69, 2005.

[23] M. Porretta, P. Nepa, G. Manara, and F. Giannetti, "Location, location, location," *IEEE Veh. Technol. Mag.*, vol. 3, no. 2, pp. 20–29, 2008.

[24] Satellite orbit determination. [Online]. Available: http://satelliteorbitdetermination.com/

[25] D. Wei and C. Y. Zhao, "Analysis on the accuracy of the SGP4/SDP4 model," *Acta Astronomica Sinica*, vol. 50, pp. 332–339, Jul. 2009.

[26] A. Yeredor and E. Angel, "Joint TDOA and FDOA estimation: A conditional bound and its use for optimally weighted localization," *IEEE Trans. Signal Process.*, vol. 59, no. 4, pp. 1612–1623, 2011.

[27] M. Leng and Y.-C. Wu, "Distributed clock synchronization for wireless sensor networks using belief propagation," *IEEE Trans. Signal Process.*, vol. 59, no. 11, pp. 5404–5414, 2011.

[28] ——, "Low-complexity maximum-likelihood estimator for clock synchronization of wireless sensor nodes under exponential delays," *IEEE Trans. Signal Process.*, vol. 59, no. 10, pp. 4860–4870, 2011.

[29] K. Römer and F. Mattern, "Towards a unified view on space and time in sensor networks," *Comput. Commun.*, vol. 28, no. 13, pp. 1484–1497, Aug. 2005.

[30] M. R. Gholami, S. Gezici, and E. G. Strom, "TDOA based positioning in the presence of unknown clock skew," *IEEE Trans. Commun.*, vol. 61, no. 6, pp. 2522–2534, 2013.

[31] B. Xu, G. Sun, R. Yu, and Z. Yang, "High-accuracy TDOA-based localization without time synchronization," *IEEE Trans. Parallel Distrib. Syst.*, vol. 24, no. 8, pp. 1567–1576, Aug 2013.

[32] O. Jean and A. J. Weiss, "Passive localization and synchronization using arbitrary signals," *IEEE Trans. Signal Process.*, vol. 62, no. 8, pp. 2143–2150, 2014.

[33] R. Rajan and A.-J. van der Veen, "Joint ranging and synchronization for an anchorless network of mobile nodes," *IEEE Trans. Signal Process.*, vol. PP, no. 99, pp. 1–16, 2015.

[34] A. Yeredor, "On passive TDOA and FDOA localization using two sensors with no time or frequency synchronization," in *Proc. IEEE Int. Conf. on Acoustics, Speech and Signal Processing*, May 2013, pp. 4066–4070.

[35] E. Tzoreff, B. Bobrovsky, and A. Weiss, "Single receiver emitter geolocation based on signal periodicity with oscillator instability," *IEEE Trans. Signal Process.*, vol. 62, no. 6, pp. 1377–1385, March 2014.

[36] Fundamentals of quartz oscillators - application note 200-2: Electronic counter series. Hewlett-Packard Company. [Online]. Available: http://literature.agilent.com/litweb/pdf/5965-7662E.pdf

[37] S. Stein, "Algorithms for ambiguity function processing," *IEEE Trans. Acoust., Speech, Signal Process.*, vol. 29, no. 3, pp. 588–599, 1981.

[38] L. Galleani and P. Tavella, "Tracking nonstationarities in clock noises using the dynamic allan variance," in *Proc. IEEE Int. Conf. on Frequency Control Symposium and Exposition*, Vancouver, BC, Aug. 2005, pp. 292–296.

[39] C. Zucca and P. Tavella, "The clock model and its relationship with the Allan and related variances," *IEEE Trans. Ultrason., Ferroelectr., Freq. Control*, vol. 52, no. 2, pp. 289–296, 2005.

[40] B. Sundararaman, U. Buy, and A. D. Kshemkalyani, "Clock synchronization for wireless sensor networks: A survey," *Ad Hoc Networks (Elsevier*, vol. 3, pp. 281–323, 2005.

[41] R. G. Gallager, *Principles of Digital Communication*. Cambridge : Cambridge University Press, 2008.

[42] M. S. Arulampalam, S. Maskell, N. Gordon, and T. Clapp, "A tutorial on particle filters for online nonlinear/non-gaussian bayesian tracking," *IEEE Trans. Signal Process.*, vol. 50, no. 2, pp. 174–188, 2002.

[43] N. Noels, H. Wymeersch, H. Steendam, and M. Moeneclaey, "True Cramer-Rao bound for timing recovery from a bandlimited linearly modulated waveform with unknown carrier phase and frequency," *IEEE Trans. Commun.*, vol. 52, no. 3, pp. 473–483, 2004.

[44] J. Chaffee, "Relating the Allan variance to the diffusion coefficients of a linear stochastic differential equation model for precision oscillators," *Ultrasonics, Ferroelectrics, and Frequency Control, IEEE Transactions on*, vol. 34, no. 6, pp. 655–658, Nov 1987.

[45] X. R. Li and V. P. Jilkov, "Survey of maneuvering target tracking. part i. dynamic models," *IEEE Trans. Aerosp. Electron. Syst.*, vol. 39, no. 4, pp. 1333–1364, 2003.

[46] Y. Bar-Shalom, X. R. Li, and T. Kirubarajan, *Estimation with applications to tracking and navigation: theory algorithms and software*. Wiley & Sons, Inc., 2001.

[47] S. M. Kay, *Fundamentals of Statistical Signal Processing: Estimation Theory*. Englewood Cliffs, NJ, 1993.

[48] F. Hlawatsch and F. Auger, Eds., *Time-Frequency Analysis: Concepts and Methods*. John Wiley & Sons, Inc., 2008.

[49] USRP N210 datasheet. Hewlett-Packard Company. [Online]. Available: http://www.ettus.com

[50] D. A. Vallado and P. Crawford, "SGP4 orbit determination," in *Proc. AIAA/AAS Astrodynamics Specialist Conference*. American Institute of Aeronautics and Astronautics, Aug. 2008, pp. 1–29.